Effective Modeling of Tunable Graphene with Dispersive FDTD - GSTC Method

Xiaofeng Du, Huan Yu, and Mengmeng Li*

Department of Communication Engineering
Nanjing University of Science and Technology, Nanjing, 210094, China
*limengmeng@njust.edu.cn

Abstract — We propose an effective method of dispersive finite difference time domain-generalized sheet transition conditions (FDTD-GSTCs) for the modeling of electromagnetic fields from tunable graphene with nearly zero thickness. To model the tunable graphene effectively, the susceptibilities are introduced instead of its physical structure, which can be extracted from reflection or transmission coefficients. In order to model the graphene in broadband, a dispersive FDTD-GSTC method is introduced by fitting the susceptibilities with respect to frequencies with the complex-conjugate pole-residue (CCPR) pairs. Numerical results demonstrate the validity of the proposed method.

Index Terms — Broadband, dispersive, finite difference time domain, grapheme.

I INTRODUCTION

Graphene has a wide range of applications due to its excellent conductivity, good thermal stability, high electron mobility, low density, promising wave absorbing material, and easy to be tunable with biasing electrostatic or a magnetostatic field [4]. To simulate it with typical three-dimensional numerical methods will lead to very low computation efficiency [5]-[10], due to its single atom thickness. To model the thin graphene layer effectively, many techniques such as the thin dielectric sheet (TDS) [5], surface impedance boundary condition [6], sub-cell discretization technique [7], and hybrid time domain implicit–explicit method [8] are widely developed.

In recent years, generalized sheet transition conditions (GSTCs) have been widely used in the analysis of electromagnetic metasurfaces [11]-[13]. In this work, we extend the GSTC for the modeling of metasurface [17] with graphene. The complex-conjugate pole-residue (CCPR) pairs method [3] is proposed to fit the dispersive susceptibility tensors for the analysis of the wideband electromagnetic property of graphene sheet.

This paper is organized as follows: Sectopm II briefly describes the FDTD-GSTC method; Section III describes the dispersive FDTD-GSTC method in detail; numerical simulations of tunable graphene in Section IV validate the proposed method. Finally, a short conclusion is given in Section V. The results of this work are initially presented at the 2018 ACES-China conference in Beijing [16].

II FDTD-GSTC METHOD

As shown in Fig. 1, the graphene is located at *xoy* plane, the boundary conditions can be written as [1], [11]:

$$\hat{z}\times\Delta\boldsymbol{H} = j\omega\boldsymbol{P}_{\parallel} - \hat{z}\times\nabla_{\parallel}M_z, \tag{1a}$$

$$\Delta\boldsymbol{E}\times\hat{z} = j\omega\mu\boldsymbol{M}_{\parallel} - \nabla_{\parallel}\left(\frac{P_z}{\varepsilon}\right)\times\hat{z}, \tag{1b}$$

$$\hat{z}\cdot\Delta\boldsymbol{D} = -\nabla\cdot\boldsymbol{P}_{\parallel}, \tag{1c}$$

$$\hat{z}\cdot\Delta\boldsymbol{B} = -\mu\nabla\cdot\boldsymbol{M}_{\parallel}, \tag{1d}$$

where $\boldsymbol{P}$ and $\boldsymbol{M}$ are the electric and magnetic surface polarization densities, respectively. $\Delta\boldsymbol{H}$ and $\Delta\boldsymbol{E}$ represent the difference of electromagnetic field on the two sides of the graphene.

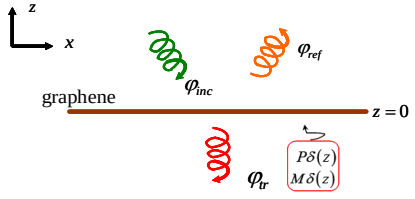

Fig. 1. Graphene located at *xoy* plane.

The electric and magnetic polarization current densities are defined as [1], [11]:

$$\boldsymbol{P} = \varepsilon\bar{\bar{\chi}}_{ee}\boldsymbol{E}_{av} + \bar{\bar{\chi}}_{em}\sqrt{\mu\varepsilon}\boldsymbol{H}_{av}, \tag{2a}$$

$$\boldsymbol{M} = \bar{\bar{\chi}}_{mm}\boldsymbol{H}_{av} + \bar{\bar{\chi}}_{me}\sqrt{\frac{\varepsilon}{\mu}}\boldsymbol{E}_{av}, \tag{2b}$$

Submitted On:October 20, 2018
Accepted On: January 26, 2019

where $\bar{\bar{\chi}}_{ee}$, $\bar{\bar{\chi}}_{em}$, $\bar{\bar{\chi}}_{me}$, and $\bar{\bar{\chi}}_{mm}$ are susceptibility tensors. $\boldsymbol{E}_{av}$ and $\boldsymbol{H}_{av}$ are the average value of electromagnetic field on the two side of the graphene.

In the particular case, we assume that the normal electric and magnetic polarization currents of graphene are zero, i.e., $P_z = 0$ and $M_z = 0$. So that the susceptibility tensors reduce to 2×2 transverse tensors. Substituting Eq. (2) into Eq. (1), we can obtain [2]:

$$\begin{pmatrix} -\Delta\tilde{H}_y \\ \Delta\tilde{H}_x \end{pmatrix} = j\omega\varepsilon \begin{pmatrix} \tilde{\chi}_{ee}^{xx} & \tilde{\chi}_{ee}^{xy} \\ \tilde{\chi}_{ee}^{yx} & \tilde{\chi}_{ee}^{yy} \end{pmatrix} \begin{pmatrix} \tilde{E}_{x,av} \\ \tilde{E}_{y,av} \end{pmatrix} + j\omega\sqrt{\mu\varepsilon} \begin{pmatrix} \tilde{\chi}_{em}^{xx} & \tilde{\chi}_{em}^{xy} \\ \tilde{\chi}_{em}^{yx} & \tilde{\chi}_{em}^{yy} \end{pmatrix} \begin{pmatrix} \tilde{H}_{x,av} \\ \tilde{H}_{y,av} \end{pmatrix}, \tag{3a}$$

$$\begin{pmatrix} \Delta\tilde{E}_y \\ -\Delta\tilde{E}_x \end{pmatrix} = j\omega\mu \begin{pmatrix} \tilde{\chi}_{mm}^{xx} & \tilde{\chi}_{mm}^{xy} \\ \tilde{\chi}_{mm}^{yx} & \tilde{\chi}_{mm}^{yy} \end{pmatrix} \begin{pmatrix} \tilde{H}_{x,av} \\ \tilde{H}_{y,av} \end{pmatrix} + j\omega\sqrt{\mu\varepsilon} \begin{pmatrix} \tilde{\chi}_{me}^{xx} & \tilde{\chi}_{me}^{xy} \\ \tilde{\chi}_{me}^{yx} & \tilde{\chi}_{me}^{yy} \end{pmatrix} \begin{pmatrix} \tilde{E}_{x,av} \\ \tilde{E}_{y,av} \end{pmatrix}, \tag{3b}$$

without loss of generality, we assume the elements are monoanisotropic and non-gyrotropic ($\tilde{\chi}_{ee}^{xy}$, $\tilde{\chi}_{ee}^{yx}$, $\tilde{\chi}_{em}^{xx}$, $\tilde{\chi}_{em}^{xy}$, $\tilde{\chi}_{em}^{yx}$, and $\tilde{\chi}_{em}^{yy}$ are equal to zero). Since the sheet is infinitesimal thin, there are no normal components of the charges and currents. As a result, the time domain expression of Eq. (3) can be simplified as:

$$J_y = \Delta H_x = \varepsilon_0 \chi_{ee}^{yy} \frac{\partial E_y}{\partial t}, \tag{4a}$$

$$J_x = \Delta H_y = \varepsilon_0 \chi_{ee}^{xx} \frac{\partial E_x}{\partial t}, \tag{4b}$$

$$K_x = \Delta E_y = \mu_0 \chi_{mm}^{xx} \frac{\partial H_x}{\partial t}, \tag{4c}$$

$$K_y = \Delta E_x = \mu_0 \chi_{mm}^{yy} \frac{\partial H_y}{\partial t}, \tag{4d}$$

where $J_p = j\omega P_p$ and $K_p = j\omega\mu_0 M_p$ with $p = x, y$ represent the polarization electric and magnetic current densities, respectively. When we insert it into the Ampere's and Faraday's laws, the FDTD updating equations as in Eq. (5) can be obtained. It can be found from Eq. (4), when the polarization susceptibilities are related to the frequencies, careful treatment of a dispersive FDTD-GSTC should be derived as will be presented in Section III.

III. DISPERSIVE FDTD-GSTC METHOD WITH CCPR PAIRS

The susceptibilitiy tensors can be extracted from the reflection and transmission coefficients [1], as a result, the susceptibility tensors are related to frequencies. In this work, the broadband susceptibilities with respect to frequencies can be fitted with the complex-conjugate pole-residue (CCPR) pairs [3]. Hence, the susceptibility tensors can be approximated as:

$$\chi(\omega) = d + \sum_{p=1}^{N} \left(\frac{c_p}{j\omega - a_p} + \frac{c_p^*}{j\omega - a_p^*} \right), \tag{6}$$

where d is a constant term, (a_p, c_p) and (a_p^*, c_p^*) are the complex-conjugate pole-residue pairs, respectively. With CCPR pairs, the polarization electric and magnetic current densities can be separated into the constant term and dispersive term:

$$\boldsymbol{J} = \boldsymbol{J}_{dis} + \boldsymbol{J}_{dis}^* + \boldsymbol{J}_{con}, \tag{7a}$$

$$\boldsymbol{K} = \boldsymbol{K}_{dis} + \boldsymbol{K}_{dis}^* + \boldsymbol{K}_{con}, \tag{7b}$$

where $\boldsymbol{J}_{con}$ and $\boldsymbol{K}_{con}$ represent constant term of electromagnetic current density. $\boldsymbol{J}_{dis}$, $\boldsymbol{J}_{dis}^*$, $\boldsymbol{K}_{dis}$ and $\boldsymbol{K}_{dis}^*$ represent two complex-conjugate pair current terms [3].

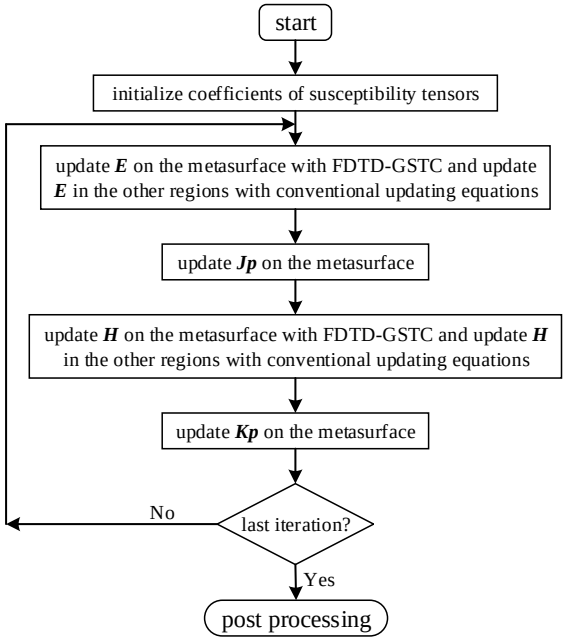

Fig. 2. A flowchart of FDTD-GSTC.

The constant term of equivalent surface currents on the graphene sheet can be solved by the traditional FDTD method [14], [15]. While the dispersive term of equivalent surface currents can be expressed by CCPR [3]:

$$\boldsymbol{J}_{p\_dis} = \varepsilon_0 \frac{c_p}{j\omega - a_p} j\omega\boldsymbol{E}, \tag{8a}$$

$$\boldsymbol{K}_{p\_dis} = \mu_0 \frac{c_{kp}}{j\omega - a_{kp}} j\omega\boldsymbol{H}. \tag{8b}$$

Assuming the graphene is located at cell of (i, j, p), Eq.

(8) in can be written in a discrete form:

$$\boldsymbol{J}_{p\_dis}^{n} = k_p \boldsymbol{J}_{p\_dis}^{n-1} + b_p \frac{\boldsymbol{E}^n - \boldsymbol{E}^{n-1}}{\Delta t}, \tag{9a}$$

$$\boldsymbol{K}_{p\_dis}^{n} = k_{kp} \boldsymbol{K}_{p\_dis}^{n-1} + b_{kp} \frac{\boldsymbol{H}^n - \boldsymbol{H}^{n-1}}{\Delta t}, \tag{9b}$$

where $k_p = \dfrac{2 + a_p \Delta t}{2 - a_p \Delta t}$, $b_p = \dfrac{\varepsilon_0 c_p 2\Delta t}{2 - a_p \Delta t}$, $k_{kp} = \dfrac{2 + a_{kp} \Delta t}{2 - a_{kp} \Delta t}$, and $b_p = \dfrac{\mu_0 c_{kp} 2\Delta t}{2 - a_{kp} \Delta t}$.

After this, we can substitute the current densities of (9) into (5), finally, the updating equation of E_y and H_y at cell (i, j, p) based on the Yee grid can be obtained as in Eqs. 10 (a) and (b). Similarly, E_x and H_x can be obtained as in Eqs. 10 (c) and (d). It should be noted here, for single layer graphene sheet without substrate $\Delta E = 0$, thus there is no need to update the magnetic equations in FDTD. The flowchart of the proposed FDTD-GSTC is shown in Fig. 2.

$$E_y^n(i,j,p) = E_y^{n-1}(i,j,p) + \frac{\Delta t}{\varepsilon_0}\left[\frac{H_x^{n-1/2}(i,j,p) - H_x^{n-1/2}(i,j,p-1)}{\Delta z} - \frac{H_z^{n-1/2}(i,j,p) - H_z^{n-1/2}(i-1,j,p)}{\Delta x}\right] - \frac{\Delta t}{\varepsilon_0}\frac{J_y(i,j,p)}{\Delta z}, \tag{5a}$$

$$H_y^{n+\frac{1}{2}}(i,j,p) = H_y^{n-\frac{1}{2}}(i,j,p) + \frac{\Delta t}{\mu_0}\left[\frac{E_z^n(i,j,p) - E_z^n(i-1,j,p)}{\Delta x} - \frac{E_x^n(i,j,p) - E_x^n(i,j,p-1)}{\Delta z}\right] - \frac{\Delta t}{\mu_0}\frac{K_y(i,j,p)}{\Delta z}, \tag{5b}$$

$$E_y^n(i,j,p) = E_y^{n-1}(i,j,p) + \frac{\Delta t}{\varepsilon_0}\frac{\varepsilon_0 \Delta z}{\varepsilon_0 \Delta z + \sum_{p=1}^{N} \mathrm{Re}(b_p) + d\varepsilon_0}\cdot\left[\frac{H_x^{n-1/2}(i,j,p) - H_x^{n-1/2}(i,j,p-1)}{\Delta z} - \frac{H_z^{n-1/2}(i,j,p) - H_z^{n-1/2}(i-1,j,p)}{\Delta x}\right]$$
$$- \frac{\Delta t}{\varepsilon_0 \Delta z}\frac{\varepsilon_0 \Delta z}{\varepsilon_0 \Delta z + \sum_{p=1}^{N} \mathrm{Re}(b_p) + d\varepsilon_0}\left[\mathrm{Re}\sum_{p=1}^{N}(1+k_p) J_{y\_dis}^{n-1}(i,j,k)\right], \tag{10a}$$

$$H_y^{n+\frac{1}{2}}(i,j,p) = H_y^{n-\frac{1}{2}}(i,j,p) + \frac{\Delta t}{\mu_0}\frac{\mu_0 \Delta z}{\mu_0 \Delta z + \sum_{p=1}^{N} \mathrm{Re}(b_{kp}) + d_k \mu_0}\cdot\left[\frac{E_z^n(i,j,p) - E_z^n(i-1,j,p)}{\Delta x} - \frac{E_x^n(i,j,p) - E_x^n(i,j,p-1)}{\Delta z}\right]$$
$$- \frac{\Delta t}{\mu_0 \Delta z}\frac{\mu_0 \Delta z}{\mu_0 \Delta z + \sum_{p=1}^{N} \mathrm{Re}(b_{kp}) + d_k \mu_0}\left[\mathrm{Re}\sum_{p=1}^{N}(1+k_{kp}) K_{y\_dis}^{n-\frac{1}{2}}(i,j,k)\right], \tag{10b}$$

$$E_x^n(i,j,p) = E_x^{n-1}(i,j,p) + \frac{\Delta t}{\varepsilon_0}\cdot\frac{\varepsilon_0 \Delta z}{\varepsilon_0 \Delta z + \sum_{p=1}^{N} \mathrm{Re}(b_p) + d\varepsilon_0}\cdot\left[\frac{H_z^{n-1/2}(i,j,p) - H_z^{n-1/2}(i,j-1,p)}{\Delta y} - \frac{H_y^{n-1/2}(i,j,p) - H_y^{n-1/2}(i,j,p-1)}{\Delta z}\right]$$
$$- \frac{\Delta t}{\varepsilon_0 \Delta z}\frac{\varepsilon_0 \Delta z}{\varepsilon_0 \Delta z + \sum_{p=1}^{N} \mathrm{Re}(b_p) + d\varepsilon_0}\left[\mathrm{Re}\sum_{p=1}^{N}(1+k_p) J_{x\_dis}^{n-1}(i,j,k)\right], \tag{10c}$$

$$H_x^{n+\frac{1}{2}}(i,j,p) = H_x^{n-\frac{1}{2}}(i,j,p) + \frac{\Delta t}{\mu_0}\frac{\mu_0 \Delta z}{\mu_0 \Delta z + \sum_{p=1}^{N} \mathrm{Re}(b_{kp}) + d_k \mu_0}\cdot\left[\frac{E_y^n(i,j,p) - E_y^n(i,j,p-1)}{\Delta z} - \frac{E_z^n(i,j,p) - E_z^n(i,j-1,p)}{\Delta y}\right]$$
$$- \frac{\Delta t}{\mu_0 \Delta z}\frac{\mu_0 \Delta z}{\mu_0 \Delta z + \sum_{p=1}^{N} \mathrm{Re}(b_{kp}) + d_k \mu_0}\left[\mathrm{Re}\sum_{p=1}^{N}(1+k_{kp}) K_{x\_dis}^{n-\frac{1}{2}}(i,j,k)\right]. \tag{10d}$$

IV NUMERICAL RESULTS

In this section, numerical simulations of graphene are shown to demonstrate the validity of the proposed dispersive FDTD-GSTC method, all the simulations are carried out on a personal computer of Intel(R) Core(TM) i3-4170 CPU with 3.7GHz and 16 GB RAM. We use Fortran to code the proposed algorithm.

A graphene with cross-shaped elements

Firstly, the graphene with cross-shaped elements is simulated, as inset in Fig. 3 (b), the dimensions of the element are: L = 48*um*, $d_1 = d_2$ = 6*um*, and the period of

the array is 60 *um*. The scattering rate of graphene sheet is 0.5 meV, the temperature is 300 K, and the biasing electric field is of 2V/nm. With the complex-conjugate pole-residue pairs method, the broadband (0.1 THz to 2 THz) susceptibilities with respect to frequencies can be fitted well as shown in Fig. 3 (a). Here, four terms are employed, and the coefficients of them are listed in Table 1, respectively.

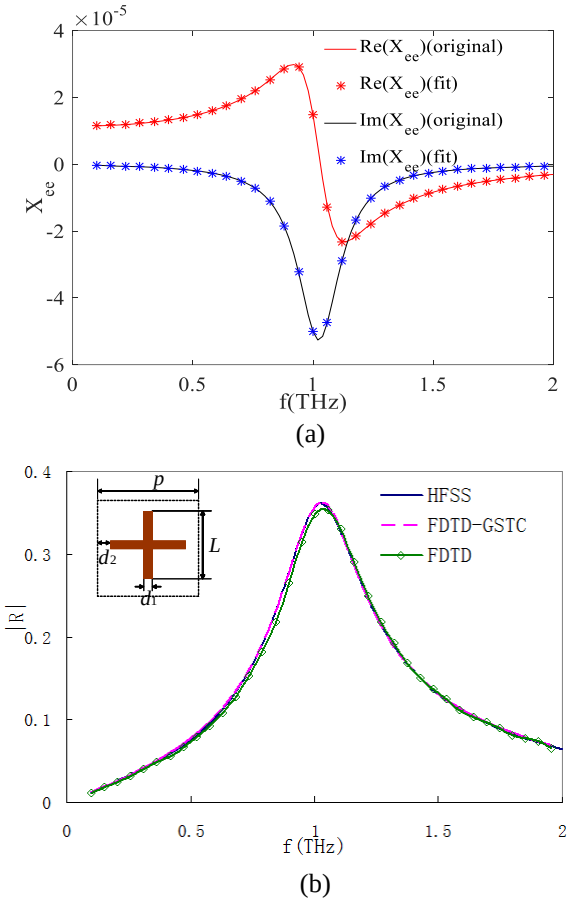

Fig. 3. Simulation of cross-shaped graphene with periodic boundary condition: (a) broadband susceptibility $\tilde{\chi}_{ee}^{xx}$ fitted by complex-conjugate pole-residue pairs, and (b) reflection coefficient by commercial software and proposed FDTD-GSTC method.

With the proposed dispersive FDTD-GSTC, the mesh size can be $dx = dy = dz = 2um$, which is much larger than conventional FDTD method [14], [15]. Figure 3 (b) plots the simulated reflection coefficients of the proposed dispersive FDTD-GSTC method and commercial software HFSS, very good agreement can be found. The simulation time and memory of FDTD and FDTD-GSTC are listed in Table 2. It can be seen that the FDTD-GSTC method requires much less number of grids and computing resources.

Table 1: Coefficients of the four terms in complex-conjugate pole-residue pairs to fit $\tilde{\chi}_{ee}^{xx} = \tilde{\chi}_{ee}^{yy}$ for the graphene sheet with cross elements (d = 4.13*e*–8)

(a_{p1}, c_{p1})	$(-1.769\times10^{12}+0j, 9.376\times10^{4}+0j)$
(a_{p2}, c_{p2})	$(-1.099\times10^{13}+0j, -4.041\times10^{6}+0j)$
(a_{p3}, c_{p3})	$(-2.866\times10^{13}+0j, 1.911\times10^{7}+0j)$
(a_{p4}, c_{p4})	$(-6.685\times10^{11}+6.217\times10^{12}j,$ $-5.575\times10^{4}-3.724\times10^{7}j)$

Table 2: Comparison of time and memory between FDTD and FDTD-GSTC

	Size of Grid (um)	Time (s)	Memory (MB)
FDTD	1×1×1	208	80
FDTD-GSTC	2×2×2	27.9	31

B graphene with asymmetrical elements

Secondly, the graphene with asymmetrical rectangular elements as inset in Fig. 4 (c) is simulated. The dimensions of the graphene element are 30*um*×18*um*, the period is 30*um*. The incident modulated Gaussian pulse is with normal propagation direction and $\hat{x}$ polarization. The scattering rate of graphene sheet is 0.96meV, the temperature is 300 K, and biasing electric field on graphene is of E = 0V/nm.

With the complex-conjugate pole-residue pairs method, the broadband (0.5 THz to 4 THz) susceptibilities $\tilde{\chi}_{ee}^{xx}$ and $\tilde{\chi}_{ee}^{yy}$ with respect to frequencies can be fitted well as shown in Figs. 4 (a) and (b). The coefficients of the four terms in complex-conjugate pole-residue pairs are listed in Tables 3 and 4.

With the proposed dispersive FDTD-GSTC, the mesh size can be $dx = dy = dz = 1um$, which is much larger than conventional FDTD method [14], [15]. The incident modulated Gaussian pulse is with normal propagation direction, Fig. 3 (c) plots the simulated reflection coefficient the proposed dispersive FDTD-GSTC method and commercial software HFSS, very good agreement can be found.

Table 3: Coefficients of the four terms in complex-conjugate pole-residue pairs to fit $\tilde{\chi}_{ee}^{xx}$ for the graphene sheet with rectangular elements (d_x = 2.94*e*–8)

(a_{p1x}, c_{p1x})	$(-3.172\times10^{10}+0j, 5.008\times10^{7}+0j)$
(a_{p2x}, c_{p2x})	$(-2.927\times10^{12}+0j, -5.269\times10^{7}+0j)$
(a_{p3x}, c_{p3x})	$(-5.9568\times10^{12}+0j, 4.524\times10^{6}+0j)$
(a_{p4x}, c_{p4x})	$(-1.141\times10^{13}+0j, -2.555\times10^{6}+0j)$
(a_{p5x}, c_{p5x})	$(-2.833\times10^{12}+3.344\times10^{13}j,$ $-4.153\times10^{5}-1.291\times10^{5}j)$

Table 4: Coefficients of the four terms in complex-conjugate pole-residue pairs to fit $\tilde{\chi}_{ee}^{yy}$ for the graphene sheet with rectangular elements ($d_y = 1.81e{-}8$)

(a_{p1y}, c_{p1y})	$(-2.341\times10^{11}+0j, 3.359\times10^{8}+0j)$
(a_{p2y}, c_{p2y})	$(-5.157\times10^{12}+0j, -4.629\times10^{7}+0j)$
(a_{p3y}, c_{p3y})	$(-1.0758\times10^{13}+0j, -2.017\times10^{7}+0j)$
(a_{p4y}, c_{p4y})	$(-1.045\times10^{12}+4.771\times10^{12}j,$ $2.147\times10^{7}-8.132\times10^{7}j)$
(a_{p5y}, c_{p5y})	$(-9.357\times10^{11}+8.878\times10^{12}j,$ $1.112\times10^{6}+2.161\times10^{6}j)$

C graphene sheet with different biasing electric fields

Thirdly, the graphene sheets with cross elements as in Section IV-A with different biasing electric fields are simulated in this part. The graphene sheet is located on the substrate with thickness of 2*um* and relative dielectric constant of 2.

As shown in Figs. 5 (a)-(c), the extracting susceptibilities ($\tilde{\chi}_{ee}^{xx} = \tilde{\chi}_{ee}^{yy}$) for the graphene sheet with biasing electrostatic field of 2 V/nm, 10 V/nm, and 20 V/nm are plotted, very good agreement between the fit and original data can be found. With the increase of static bias electric field, the peaks of reflection coefficient also gradually increase and shift to the high frequency regime as in Fig. 5 (d).

D turntable graphene sheet array

The last simulation example is a finite size graphene sheet composed of 10×10 cross elements as in Fig. 6. The observed frequencies are chosen at which the largest reflection occur, e.g., 0.9 THz, 1.18 THz, and 1.5 THz, respectively. The bistatic RCS is calculated by FDTD-GSTC and HFSS. It can be found that the results of the proposed method are in good agreement with the commercial software, while our proposed method is much more efficient as listed in Table 5.

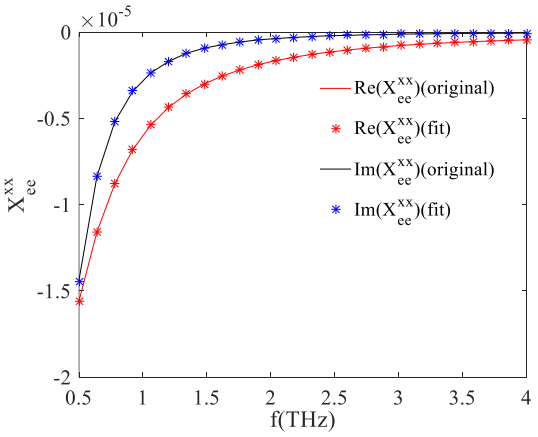

(a)

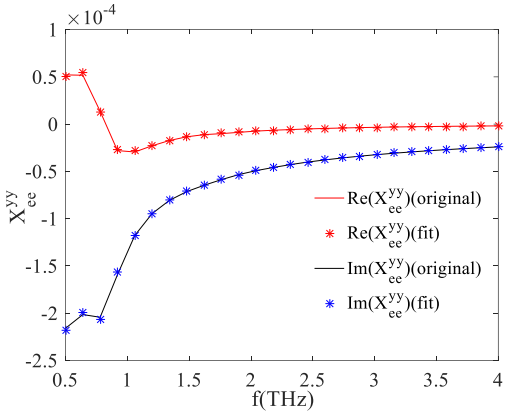

(b)

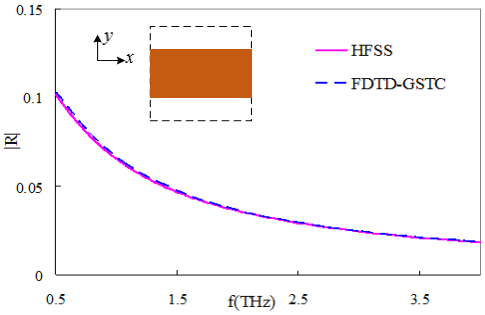

(c)

Fig. 4. Simulation of asymmetrical graphene sheet with rectangular elements: (a) extracted susceptibility $\tilde{\chi}_{ee}^{xx}$, (b) extracted susceptibility $\tilde{\chi}_{ee}^{yy}$, and (c) reflection coefficient by commercial software and proposed FDTD-GSTC method.

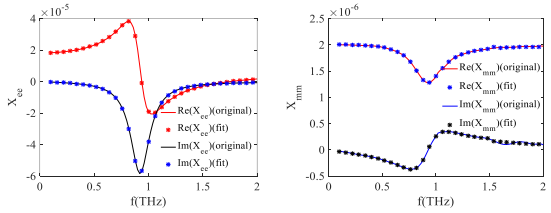

(a)

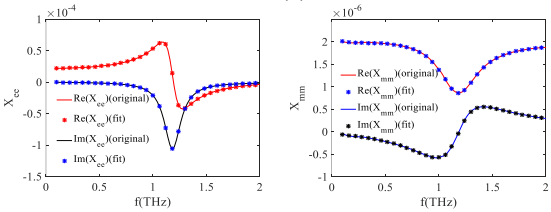

(b)

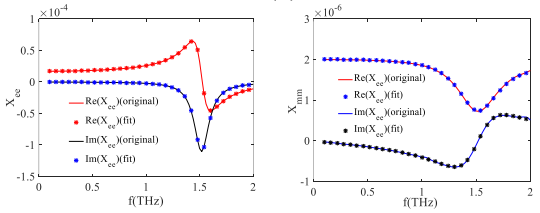

(c)

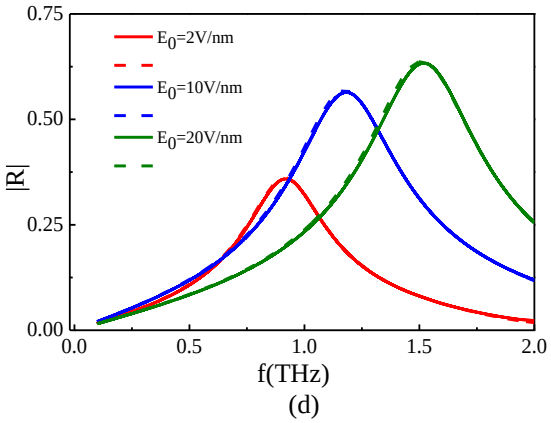

Fig. 5. Simulation of the graphene sheet with different biasing electric field: (a) susceptibilities when E = 2V/nm, (b) susceptibilities when E = 10V/nm, (c) susceptibilities when E = 20V/nm, and (d) reflection coefficients with different static biasing electric fields.

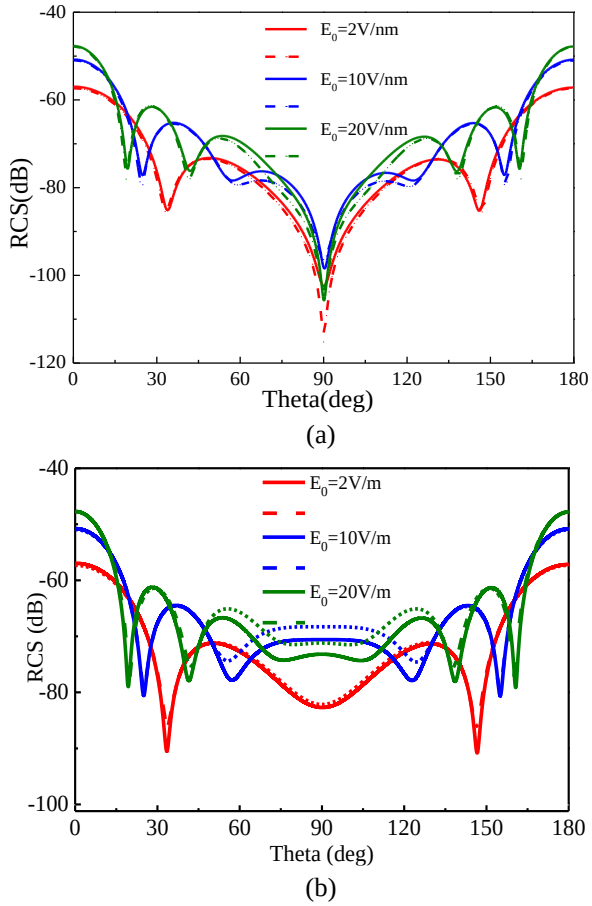

Fig. 6. Validation: bistatic RCS of finite graphene sheet composed of 10×10 cross computed by HFSS (solid line) and FDTD-GSTC (dotted line).

Table 5: Comparison of time and memory between HFSS and FDTD-GSTC

Method	Number of Elements	Time (hh:mm:ss)	Memory (GB)
HFSS	7290500	38:51:39	32
FDTD-GSTC	398×398×99	07:49:51	12

V. CONCLUSION

We proposed an effective dispersive FDTD-GSTC method to analyze the electromagnetic property of graphene by using the complex-conjugate pole-residue pairs. Typical tunable graphene sheets with cross and rectangular elements are simulated in a broadband. The accuracy of the method and the computation performance is validated with respect to commercial software.

ACKNOWLEDGMENT

This work is partially supported by Natural Science Foundation of China (61871222, 61507237); Natural Science Foundation of Jiangsu Province (BK20171429); Fundamental Research Funds for the Central Universities (30918011103).

REFERENCES

[1] K. Achouri, M. A. Salem, and C. Caloz, "General metasurface synthesis based on susceptibility tensors," *IEEE Trans. Antennas Propag.*, vol. 63, no. 7, pp. 2977-2991, July 2015.

[2] Y. Vahabzadeh, N. Chamanara, K. Achouri, et al., "Computational analysis of metasurfaces," *IEEE Journal on Multiscale and Multiphysics Computational Techniques*, vol. 3, pp. 37-49, Apr. 2018.

[3] M. Han, R. W. Dutton, and S. Fan, "Model dispersive media in finite-difference time-domain method with complex-conjugate pole-residue pairs," *IEEE Microw. Wireless Compon. Lett.*, vol. 16, no, 3, pp. 119-121, 2006.

[4] A. Geim and K. Novoselov "The rise of graphene," *Nature Mater.*, vol. 6, pp. 183-191, 2007.

[5] Y. Zhao, S. Tao, D. Ding, et al., "A time-domain thin dielectric sheet (TD-TDS) integral equation method for scattering characteristics of tunable graphene," *IEEE Trans. Antennas Propag.*, vol. 66, no, 3, pp. 1366-1373, Jan. 2018.

[6] J. C. Mak and C. D. Sarris, "A surface impedance boundary condition approach to the FDTD modeling of graphene," *IEEE Antennas and Propagation Society International Symposium (APSURSI)*, pp.902-903, July 2013.

[7] X. Yu and C. D. Sarris, "A perfectly matched layer for subcell FDTD and applications to the modeling of graphene structures," *IEEE Antennas Wireless Propag. Lett.*, vol. 11, no. 4, pp. 1080-1083, 2012.

[8] J. Chen, N. Xu, A. Zhang, et al., "Using dispersion HIE-FDTD method to simulate the graphene-based polarizer," *IEEE Trans. Antennas Propag*., vol. 24, no. 7, pp. 3011-3017, July 2016.

[9] A. Eldek, A. Z. Elsherbeni, and C. E. Smith, "Analysis of transmission and reflection from modified coplanar waveguide structures," *ACES Journal*, vol. 17, no. 2, pp. 158-165, July 2002.

[10] M. Li, C. Xia, and R. Chen, "Full-wave analysis of microstrip circuits with reciprocal matrix compression technique," *ACES Journal*, vol. 31, no. 1382-1388, Dec. 2016.

[11] E. F. Kuester, M. A. Mohamed, M. Piket-May, et al., "Averaged transition conditions for electromagnetic fields at a metafilm," *IEEE Trans. Antennas Propag.*, vol.51, no.10, pp. 2641-2651, 2003.

[12] X. Jia, X. Liu, F. Yang, et al., "An accelerated method of metasurfaces simulation by introducing susceptibilities into FDTD based on GSTCs," *arXiv* preprint *arXiv*:1710.09193, 2017.

[13] Y. Vahabzadeh, N. Chamanara, and C. Caloz "Generalized sheet transition condition FDTD simulation of metasurface," *IEEE Trans. Antennas Propag.*, vol. 66, no. 1, pp. 271-280, 2018.

[14] H. Bao and R. Chen, "An efficient domain decomposition parallel scheme for leapfrog ADI-FDTD method," *IEEE Trans. Antennas Propag*., vol. 65, no. 3, pp. 1490-1494, Mar. 2017

[15] H. Bao, D. Z. Ding, and R. S. Chen, "A hybrid spectral-element finite-difference time-domain method for electromagnetic simulation," *IEEE Antennas Wireless Propag. Lett*., vol. 16, pp. 2244-2248, 2017.

[16] X. Du, H. Yu, M. Li, and R. S. Chen, "Simulation of all dielectric metasurafce with finite thickness based on FDTD-GSTC," *2018 ACES-China Conference*, pp. 1-2, July 29-Aug. 1, 2018.

[17] M. Li, S. Li, Y. Yu, X. Ni, and R. Chen, "Design of random and sparse metalens with matrix pencil method," *Optics Express*, vol. 26, no. 19, pp. 24702-11, Sep. 2018.

Xiaofeng Du received the B.S. degree in Electrical Engineering from the Hefei University of Technology, Xuancheng, China, in 2016. She is pursuing the master degree in Electromagnetic Field and Microwave Technology in the Nanjing University of Science and Technology, Nanjing, China. Her current research interest is effective FDTD modeling of tunable metasurface.

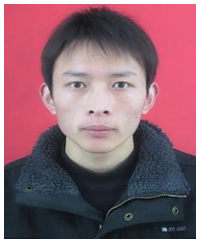

Mengmeng Li received the B.S. degree (Hons.) in Physics from Huaiyin Normal College, Huai'an, China, in 2007, and the Ph.D. degree in Electromagnetic Field and Microwave Technology from Nanjing University of Science and Technology, Nanjing, China, in 2014. From 2012 to 2014, he was a Visiting Student with the Electronics Department, Politecnico di Torino, Turin, Italy. Since 2014, he has been with the Department of Communication Engineering, Nanjing University of Science and Technology, where he has been an Associate Professor since 2017. In 2017, he was a Visiting Scholar with Pennsylvania State University, Pennsylvania, PA, USA. His current research interests include fast solver algorithms and multiscale simulations.

Li was a recipient of the Doctoral Dissertation Award of Jiangsu in 2016, the Student Paper Award at the International Conference on Microwave and Millimeter Wave Technology in 2012. He serves as an active Reviewer for the IEEE Journals and Conferences, and has been an Associate Editor for the IEEE Access.